Supplementary Materials

A. Determination of Refractive Index

To retrieve the refractive index of the samples with varying Au volume fraction, we performed the angle dependent reflectance measurement for the two principal polarisation, as shown in Fig. S5.

We applied a generalised transfer matrix method that was developed by Yeh[1] to derive the optical constants from the reflectometry measurements. It is known that np-Si has anisotropic properties with its crystal axis aligned along the direction of silicon etching[2]. In the cartesian coordinate system, where we chose xz as the incident plane with wave propagating along z direction, the np-Si permittivity tensor can be expressed as

$$\overleftrightarrow{\epsilon} = \begin{bmatrix} \epsilon_o & 0 & 0 \\ 0 & \epsilon_o & 0 \\ 0 & 0 & \epsilon_e \end{bmatrix} , \quad (1)$$

where ϵ_o and ϵ_e are the complex ordinary and extra-ordinary permittivity, respectively. By implementing the permittivity tensor and solving the wave equation

$$\vec{k} \times (\vec{k} \times \vec{E}) + {k_0}^2 \overleftrightarrow{\epsilon} \vec{E} = 0 , \quad (2)$$

with $k_0 = \omega/c$. Four wave propagating modes can be obtained which have the same x component $\vec{k}_x = k_0 \sin\theta$ (θ is the incident angle), but different z component of wave vectors for ordinary and ex-ordinary wave, $\vec{k}_{oz}$ and $\vec{k}_{ez}$, respectively:

$$\vec{k}_{oz} = \pm\sqrt{k_0^2\epsilon_o - \vec{k}_x^2} , \quad (3)$$

$$\vec{k}_{ez} = \pm\sqrt{(k_0^2 - \frac{\vec{k}_x^2}{\epsilon_e})\epsilon_o} . \quad (4)$$

Here, '±' denotes the direction of the wave propagation (forward and backward). Further, the corresponding electric field polarisation directions can be determined as

$$\vec{p}_o = \vec{k}_o \times \vec{z} , \quad (5)$$

$$\vec{p}_e = \overleftrightarrow{\epsilon}^{-1} \times \vec{k}_e \times \vec{y} , \quad (6)$$

where $\vec{y}$ and $\vec{z}$ are the unit vector perpendicular to the plane of incidence and parallel to the surface normal, respectively.

Afterwards, the reflection coefficient for s- and p- components, r_s and r_p, of the anisotropic np-Si layer on top of the bulk Si substrate can be simulated to fit the experimental results, by applying the generalised 4×4 transfer matrix method developed by P. Yeh[1]:

$$r_s = \frac{M(2,1)M(3,3) - M(2,3)M(3,1))}{M(1,1)M(3,3) - M(1,3)M(3,1)} \ , \tag{7}$$

$$r_p = \frac{M(1,1)M(4,3) - M(4,1)M(1,3))}{M(1,1)M(3,3) - M(1,3)M(3,1)} \ , \tag{8}$$

where the system transfer matrix is defined by $M = D_{air}{}^{-1} D_{np-Si} P_{np-Si} D_{np-Si}{}^{-1} D_{Si}$. Here D represents the dynamic matrix which only depends on the polarisation of the incidence light:

$$D = \begin{bmatrix} \vec{p_o}\vec{x} & \vec{p_o'}\vec{x} & \vec{p_e}\vec{x} & \vec{p_e'}\vec{x} \\ \vec{q_o}\vec{y} & \vec{q_o'}\vec{y} & \vec{q_e}\vec{y} & \vec{q_e'}\vec{y} \\ \vec{p_o}\vec{y} & \vec{p_o'}\vec{y} & \vec{p_e}\vec{y} & \vec{p_e'}\vec{y} \\ \vec{q_o}\vec{x} & \vec{q_o'}\vec{x} & \vec{q_e}\vec{x} & \vec{q_e'}\vec{x} \end{bmatrix} \ , \tag{9}$$

the polarisation vectors $\vec{p_o}$ and $\vec{p_e}$ are as defined in eq.(5) and eq.(6) for forward propagation and $\vec{p_o}'$ and $\vec{p_e}'$ for backward propagation, with the same x but opposite z components relative to the forward mode. $\vec{q_o}$ and $\vec{q_e}$ are the magnetic field polarisation vectors which are related to the electric field polarisation vectors by $\vec{q} = \frac{1}{\omega}\vec{k} \times \vec{p}$. In addition, P_{np-Si} is the propagating matrix which only depends on the phase change induced by the anisotropic layer:

$$P_{np-Si} = \begin{bmatrix} exp(-ik_{oz}z) & 0 & 0 & 0 \\ 0 & exp(ik_{oz}z) & 0 & 0 \\ 0 & 0 & exp(-ik_{ez}z) & 0 \\ 0 & 0 & 0 & exp(ik_{ez}z) \end{bmatrix} \ , \tag{10}$$

where z is the thickness of the anisotropic layer. More details about the generalised transfer matrix method can be found elsewhere[3,4]. Finally, r_s and r_p are used to calculate the absolute reflectance given by $R_0 = |r|^2$ as well as its pump-induced change $\Delta R/R_0$.

The retrieved optical constants of the real and imaginary parts, ϵ_r and ϵ_i, of the effective dielectric function of np-Si/Au composite and their evolution as the clusters volume fraction increases from 0 to 0.13 are displayed in Fig. S6. Each part of the dielectric function is contributed by the ordinary and extraordinary components arising from the weak uniaxial birefringence of the np-Si matrix. It can be seen that at the higher cluster densities, the randomness of their distribution seems to negate the birefringence effect. The refractive index was then obtained by taking the square root of the dielectric function. We note that laser with 2.5 μm wavelength was used in the reflectance measurement. The mean purpose of the measurement was to obtain the effective dielectric function and use it to further calculate the Au volume fraction (introduced in next subsection).

B. Au Volumetric Fraction, f_{Au}, Estimation

After extracting the complex dielectric function of np-Si layer immersed in gold solutions for different periods of time. 2D Maxwell Garnett Mixing Formula[5] was applied to estimate the volume fraction, f_{Au}, of Au clusters:

$$\frac{\epsilon_{eff} - \epsilon_{air}}{\epsilon_{eff} + \epsilon_{air}} = f_{Si}\frac{\epsilon_{Si} - \epsilon_{air}}{\epsilon_{Si} + \epsilon_{air}} + f_{Au}\frac{\epsilon_{Au} - \epsilon_{air}}{\epsilon_{Au} + \epsilon_{air}} \tag{11}$$

where $\epsilon_{Air} = 1$, $\epsilon_{eff}^2 = \epsilon_o^2 + \epsilon_e^2$ represents the effective dielectric constant of np-Si/Au sample obtained from the reflectometry measurements; ϵ_{Si} and ϵ_{Au} are the dielectric functions of Silicon[2] and Gold[6], respectively. The volume fraction of silicon $f_{Si} = 0.35$ was estimated from the gravimetric method as mentioned above. After solving Eq. 11, we worked out f_{Au} for sample np-Si/Au 1 - 4, which is 0.02, 0.05, 0.08 and 0.13($\pm$ 0.02), respectively.

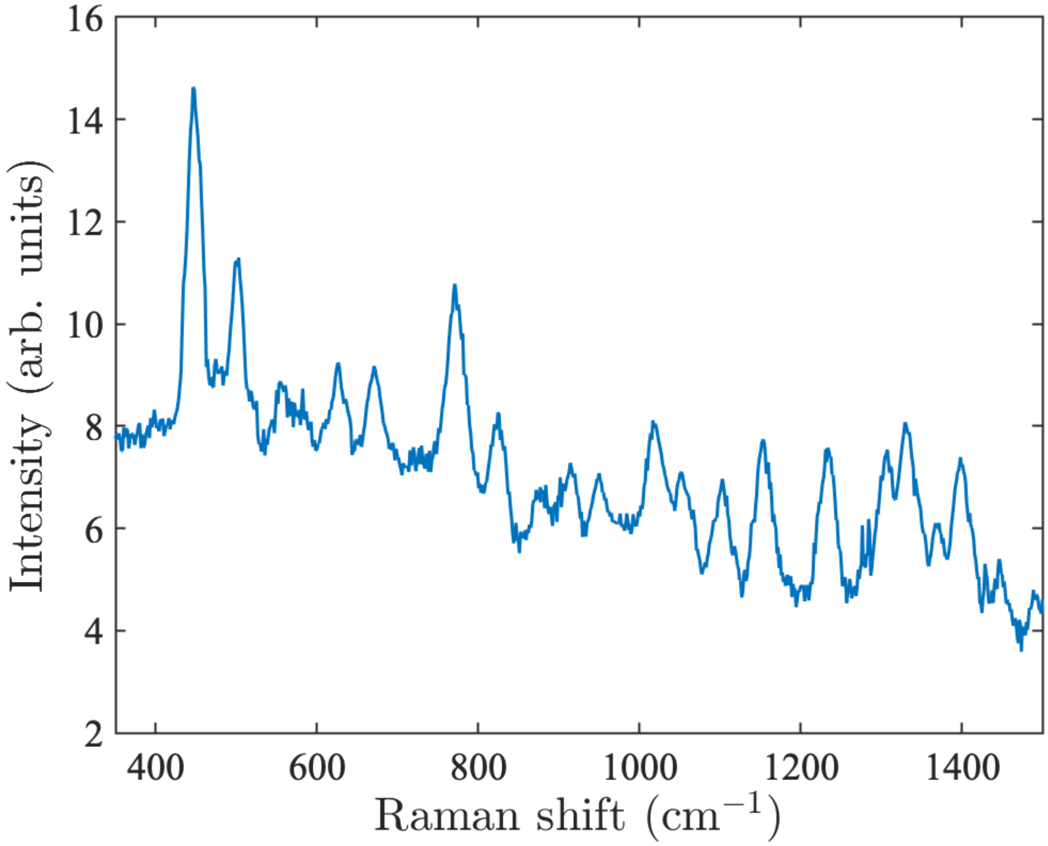

FIG. S1. The Raman spectrum of 100 mM MB on the smooth Au film.

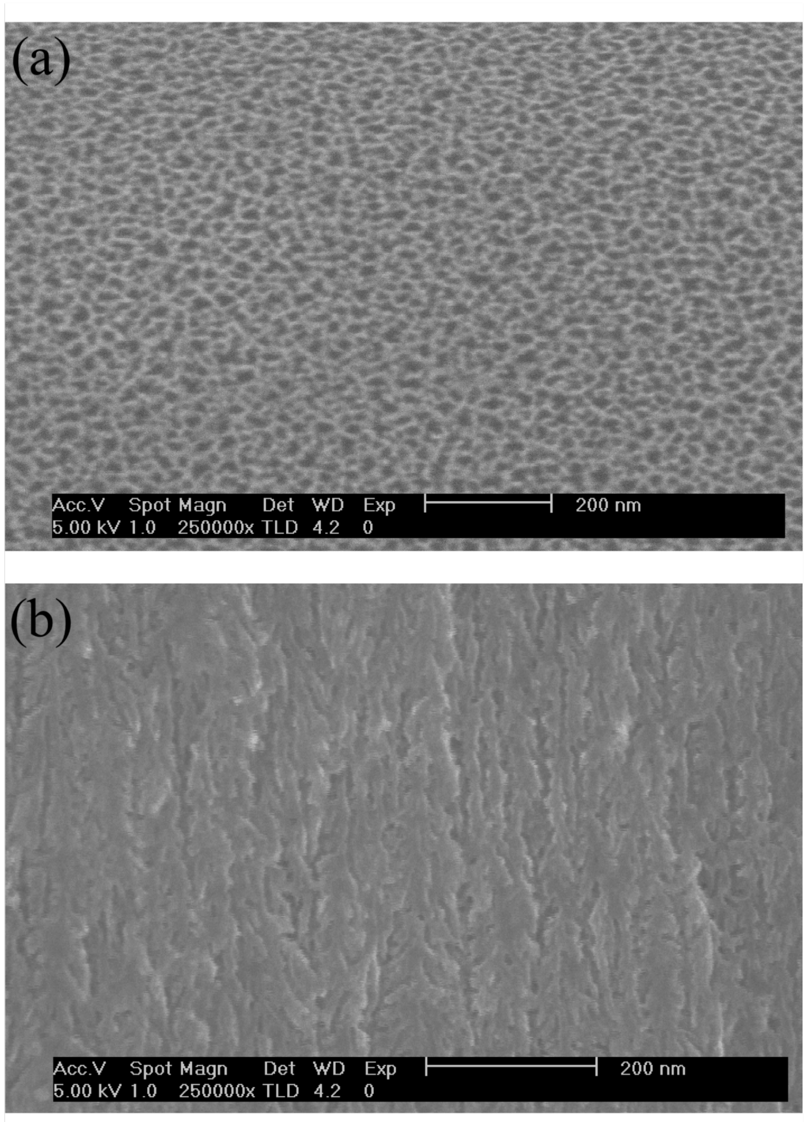

FIG. S2. SEM top (a) and cross-section (b) image of np-Si before Au impregnation.

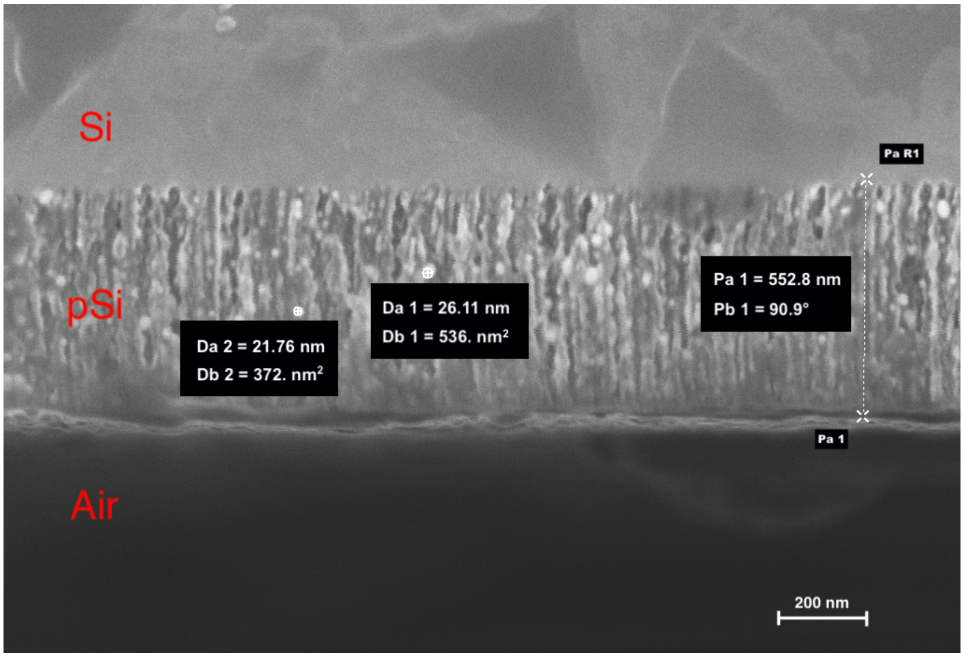

FIG. S3. SEM cross-section image of np-Si+0.02 Au. The labels show the diameter (Da) and area (Db) of the selected Au clusters and the thickness (Pa) of the pSi layer.

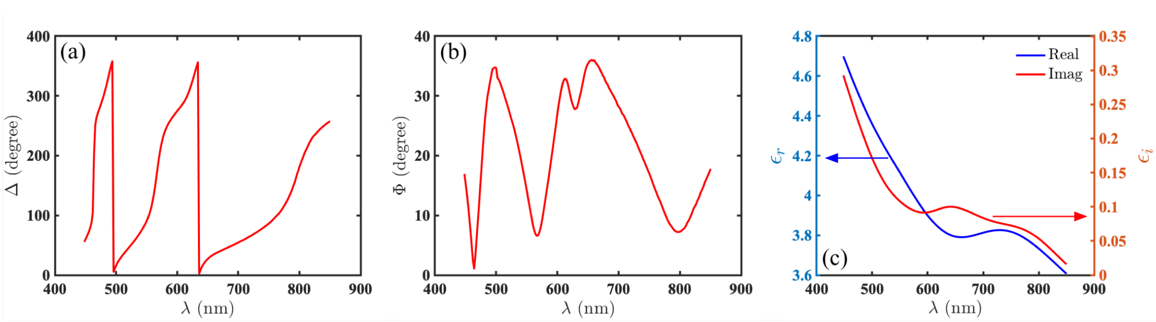

FIG. S4. Spectroscopic ellipsometry results of np-Si without Au clusters (a-b), and the retrieved complex dielectric function (c).

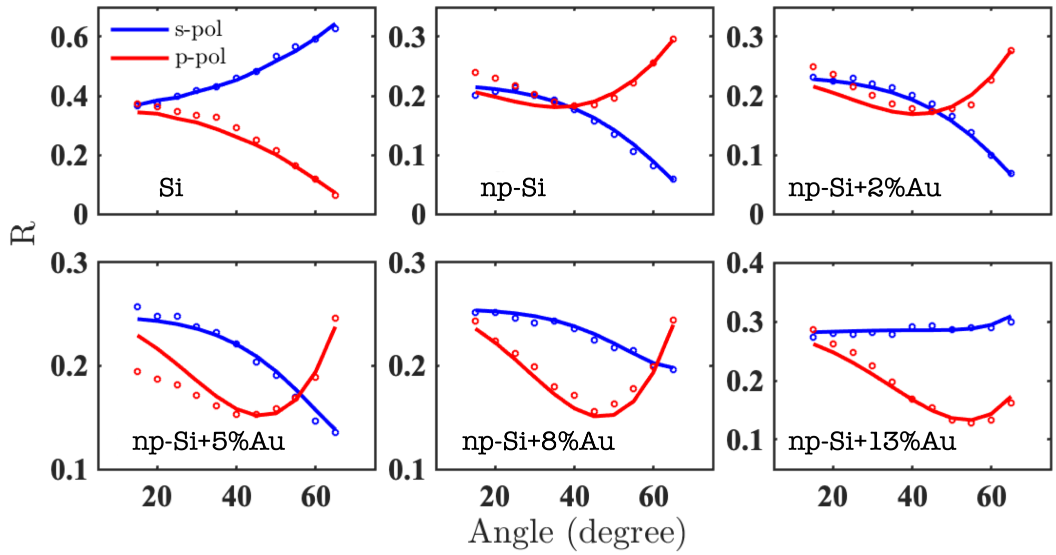

FIG. S5. The angular dependence of the reflectance, R, for s- and p-polarisation measured on bulk silicon (left top) and np-Si with different fraction of Au clusters, the solid lines are the model t.

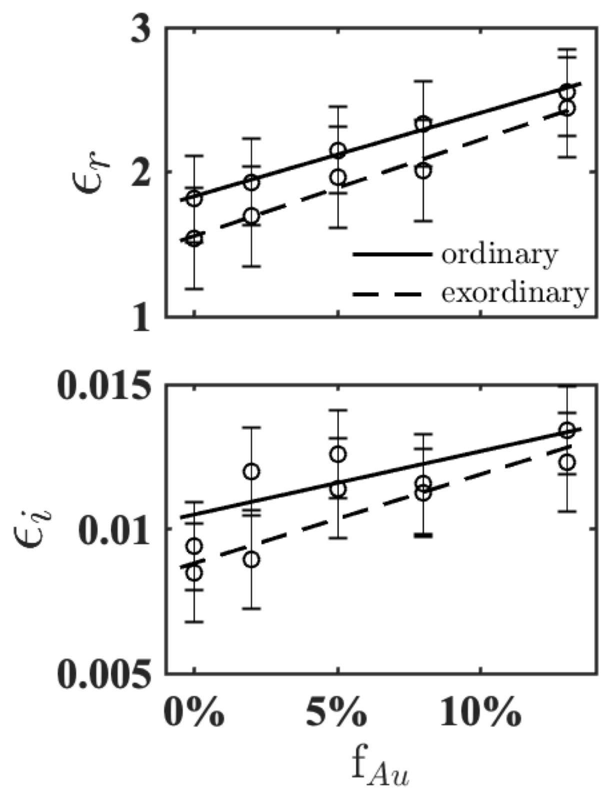

FIG. S6. The effective real and imaginary part of the dielectric function, ϵ_r and ϵ_i, as a function of Au volume fraction.

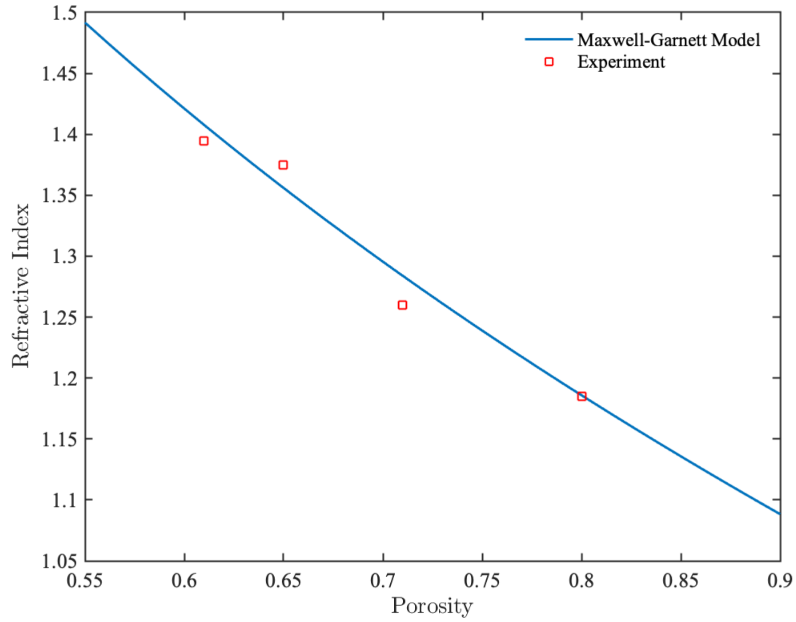

FIG. S7. Refractive index of np-Si as a function of the porosity. The solid line represents Maxwell-Garnett Model, the squares denote experimental results.

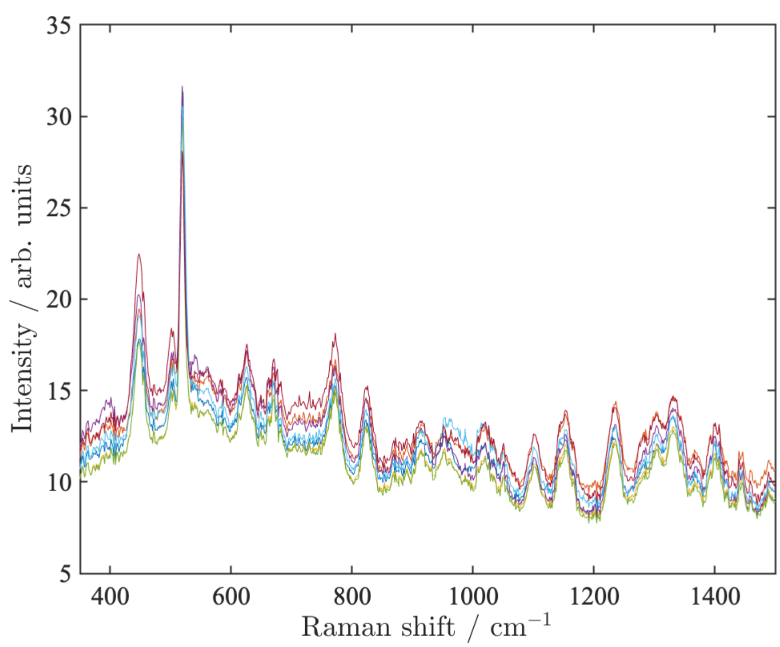

FIG. S8. Reproducibility of Raman spectrum of 1 μM MB measured across a few centimetres at random locations on np-Si+0.02 Au.

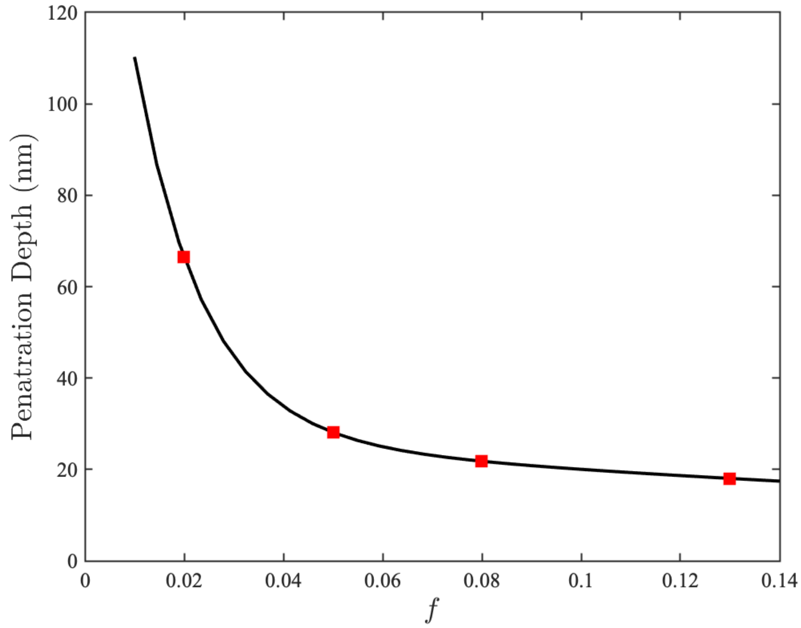

FIG. S9. Optical penetration depth of 800 nm laser as a function of Au volume fraction, f.

REFERENCES

[1]P. Yeh, "Optics of anisotropic layered media: a new 4× 4 matrix algebra," Surface Science **96**, 41–53 (1980).

[2]V. Y. Timoshenko, L. Osminkina, A. Efimova, L. Golovan, P. Kashkarov, D. Kovalev, N. Künzner, E. Gross, J. Diener, and F. Koch, "Anisotropy of optical absorption in birefringent porous silicon," Physical Review B **67**, 113405 (2003).

[3]P. Yeh, "Electromagnetic propagation in birefringent layered media," JOSA **69**, 742–756 (1979).

[4]P. Yeh, "Extended jones matrix method," JOSA **72**, 507–513 (1982).

[5]A. Zakar, R. Wu, D. Chekulaev, V. Zerova, W. He, L. Canham, and A. Kaplan, "Carrier dynamics and surface vibration-assisted auger recombination in porous silicon," Physical Review B **97**, 155203 (2018).

[6]A. D. Rakić, A. B. Djurišić, J. M. Elazar, and M. L. Majewski, "Optical properties of metallic films for vertical-cavity optoelectronic devices," Applied optics **37**, 5271–5283 (1998).

[7]R. Wu, J. Collins, D. Chekulaev, and A. Kaplan, "All-optical modulation and ultrafast switching in mwir with sub-wavelength structured silicon," Applied Sciences **9**, 1808 (2019).

[8]R. Wu, J. Collins, L. Canham, and A. Kaplan, "The influence of quantum confinement on third-order nonlinearities in porous silicon thin films," Applied Sciences **8**, 1810 (2018).

[9]C. Schinke, P. Christian Peest, J. Schmidt, R. Brendel, K. Bothe, M. R. Vogt, I. Kröger, S. Winter, A. Schirmacher, S. Lim, *et al.*, "Uncertainty analysis for the coefficient of band-to-band absorption of crystalline silicon," Aip Advances **5**, 067168 (2015).